Effects of drainage conditions and suction pressure on tensile response of bucket foundations

An experimental study

Grecu, Sorin; Ibsen, Lars Bo; Barari, Amin

Published in:
Ocean Engineering

DOI (link to publication from Publisher):
10.1016/j.oceaneng.2023.114277

Publication date:
2023

Document Version
Publisher's PDF, also known as Version of record

Ocean Engineering 277 (2023) 114277

Contents lists available at ScienceDirect

Ocean Engineering

journal homepage: www.elsevier.com/locate/oceaneng

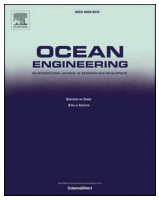

Effects of drainage conditions and suction pressure on tensile response of bucket foundations: An experimental study

Sorin Grecu [a,*], Lars Bo Ibsen [a], Amin Barari [a,b]

[a] Department of the Built Environment, Aalborg University, Thomas Manns Vej 23, Aalborg East, 9220, Denmark
[b] School of Engineering, RMIT University, Melbourne, VIC, 3000, Australia

ARTICLE INFO

Handling Editor: Prof. A.I. Incecik

Keywords:
Suction bucket
Offshore foundation
Uplift
Tensile capacity
Stiffness

ABSTRACT

Suction buckets acting as supports for jacket structures may constitute a viable foundation solution for offshore wind turbines. While monopiles dominate the industry, suction buckets remain uncommon despite their advantages in transitional water depths. One of the reasons stems from challenges of achieving optimal design due to scarce experience and knowledge, as the mechanisms governing foundation response to different drainage conditions are poorly understood. This paper contributes with new insights into tensile behavior of suction buckets based on experimental evidence. A defining property of bucket foundations is the ability to withstand extreme uplift forces on account of suction, which represents the core subject of this study. All tests involved a medium-scale model installed in sand in a pressurized environment. A novel feature of this research consists of examining the relative importance of soil density. By varying the relative density (40–90%) and the uplift rate (0.05–500 mm/s), a full range of drainage and soil conditions was explored. Suction pressure generated during partially drained or fully undrained uplift tends to reach similar values regardless of initial relative density. This key finding demonstrates how the soil state is altered due to jacking installation and cyclic pre-shearing. Regression models are established to capture the dependency of tensile capacity and initial stiffness on uplift rate.

1. Introduction

The suction bucket jacket (SBJ) system is illustrated in Fig. 1. Given a sufficiently large overturning moment, windward buckets experience tensile loading, while the leeward ones become subjected to additional compression. Resistance to uplift forces represents an essential factor in ensuring safe and serviceable design, but predicting it accurately is still a topic in development.

The first instance of a full-scale SBJ was the Draupner platform, installed in dense sand in the North Sea near the Norwegian coast (Tjelta, 2015). What really put it in the spotlight was the recording of a rare natural occurrence: an unusually large wave that imposed extreme loads on the foundation. No failure happened, and thus the SBJ concept became validated in severe field conditions. In their analysis of the event, Hansteen et al. (2003) estimated the maximum applied uplift load at less than half of the design vertical capacity. This reflects the degree of conservatism which was necessary to tackle the uncertainties of a novel concept.

Within the offshore wind industry, the monopile technology comes as the standard foundation solution, while SBJs form a niche that steadily garners interest, particularly when larger water depth is involved. The first ever SBJ supporting a wind turbine was installed at Borkum Riffgrund 1 wind farm in 2014 (Shonberg et al., 2017). Since then, this foundation type was deployed at Borkum Riffgrund 2 and Aberdeen Bay offshore wind farms (OWF). Furthermore, Seagreen OWF, which is in development at the time of writing, will use SBJs to support all of its 114 turbines. The given list is not exhaustive.

Another advance in the field is the issuing of a design guide by The Carbon Trust (Cathie et al., 2019), in which the guidelines for estimating tensile response are based on experimental evidence. The report proposes simple calculation methods for drained and undrained analyses, stating that partially drained approaches require site-specific assessment. This is not unexpected, since predicting partially drained conditions implies additional complexities that have not yet been addressed in a general design framework. The present study invokes this fact as one of its sources of motivation and explores the full spectrum of drainage modes.

Existing experimental work on tensile behavior of suction buckets

* Corresponding author.
E-mail address: sgre@build.aau.dk (S. Grecu).

https://doi.org/10.1016/j.oceaneng.2023.114277
Received 29 December 2022; Received in revised form 7 February 2023; Accepted 19 March 2023
Available online 31 March 2023

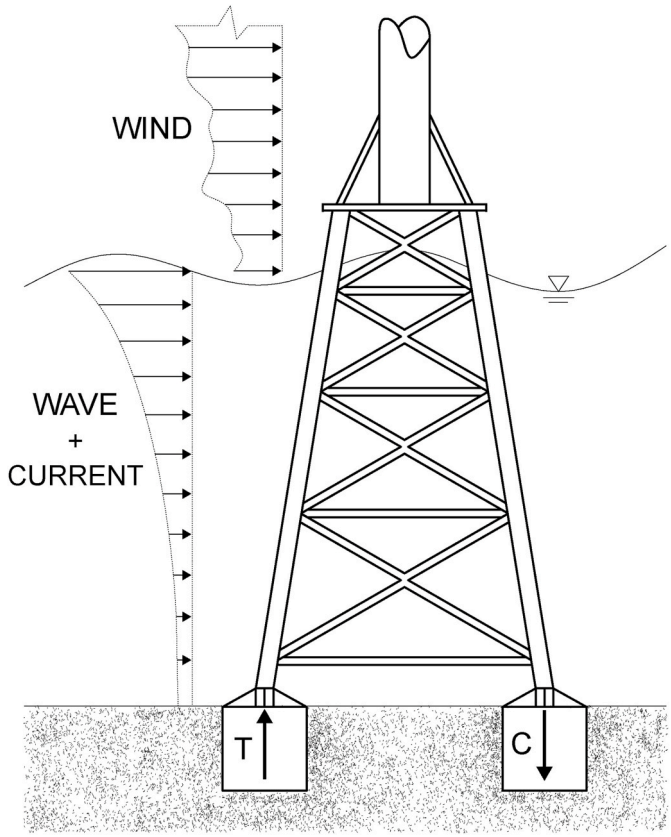

Fig. 1. Conceptual sketch of an SBJ acting as foundation for a wind turbine, where T and C stand for "tension" and "compression", respectively (adapted from Grecu et al., 2021).

can be classified according to simulated gravity conditions into *1* g and *N*g tests. Some studies associated with the latter category are reported by Chen and Randolph (2007); Acosta-Martinez et al. (2008); Mana et al. (2011); Acosta-Martinez et al. (2012); Mana et al. (2012, 2013a,b); Koh et al. (2017); Wang et al. (2018, 2019); Jeong et al. (2020); Zhao et al. The 1 g group can be further divided into tests conducted in open containers (Byrne and Houlsby, 2002; Kelly et al., 2004; Luke et al., 2005; Kakasoltani et al., 2011; Gütz et al., 2017; Vaitkune et al., 2017; Kulczykowski, 2020; Vicent et al., 2020, 2021) and in closed pressurized environments (Kelly et al., 2006; Vaitkunaite et al., 2016). All experiments presented here were carried out in a pressure tank. The use of additional ambient pressure brings two benefits in terms of modelling offshore foundations. Firstly, entrapped air bubbles are compressed or forced out of soil, thus further ensuring full saturation. Secondly, it makes it possible to simulate any water depth. This is especially relevant when loading suction buckets in tension, since cavitation defines the possible amount of excess pore pressure, as explained by Thieken et al. (2014).

The review of published research identified general lack of consideration of density as a factor in vertical response of suction buckets. Thus, the current study aims to fill this gap by gaining insight into the influence of sand density. Additionally, it sets to further investigate the relationship between uplift rate and tensile behavior. To accomplish these, relative density and uplift rate comprise the controlled independent variables of the testing campaign. Another distinguishing trait of this research is the inclusion of a cyclic pre-shearing procedure, with the goal of analyzing possible impact of force cycles on foundation response during an extreme event.

The experimental campaign involves 23 tests. The choice of values of independent variables allows examining their contributions separately, as well as identifying potential interaction effects. The uplift rates range from 0.05 to 500 mm/s and relative densities vary between 40 and 90%. The response variables consist of vertical force at the bucket lid's center and pore pressure at 12 discrete points distributed on both skirt sides and beneath the lid.

2. Experimental arrangement

This section provides detailed descriptions of all pieces of equipment and materials involved in the experimental campaign. At no point during testing was the limit of any device or material exceeded. Checks and necessary recalibrations were performed on all sensors before each test.

2.1. Pressure tank

The tank has a cylindrical shape and is made of steel. Fig. 2 outlines only the details that are considered relevant to understanding and reproducing this research. Both inner diameter and height measure 2.1 m. The soil is composed of a 0.6 m layer of sand on top of 0.3 m of gravel. A permeable membrane separates the two layers.

An MTS 244G2 hydraulic actuator was employed to generate loads, which were read by a load cell. The actuator has an internally mounted LVDT for monitoring displacement. All data, including signals from pressure transducers, was recorded with an MTS FlexDAC 20 acquisition system.

Vaitkunaite et al. (2016) and Nielsen et al. (2017) conducted tests on suction bucket models in the same tank, but used different actuating, measuring and data acquiring devices than the ones described here.

2.2. Foundation model

The model parameters are summarized in Table 1. The bucket mass includes the contribution of all the transducers and attachments. The skirt length to lid diameter ratio (L/D) is taken as unity, even though it equals 1.02 precisely.

The steel bucket model (Fig. 3) is equipped with 12 pressure transducers that are attached to columns mounted on the lid. They measure pressure at different points on the bucket surface via thin metal tubes

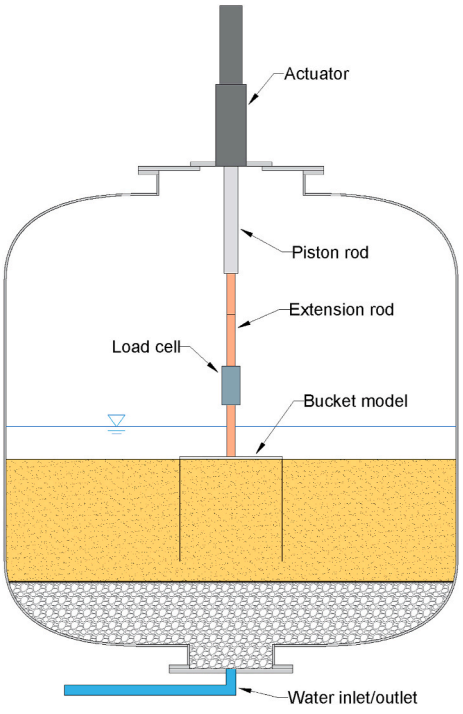

Fig. 2. Sketch of the pressure tank. Only the essential details are depicted.

Table 1
Model parameters.

Parameter name (Symbol)	Value	Unit
Outer diameter (D_o)	500	mm
Inner diameter (D_i)	492	mm
Outer skirt length (L_o)	510	mm
Inner skirt length (L_i)	498	mm
Lid plate thickness (t_{lid})	12	mm
Skirt plate thickness (t_{skirt})	4	mm
Mass (m)	65.24	kg

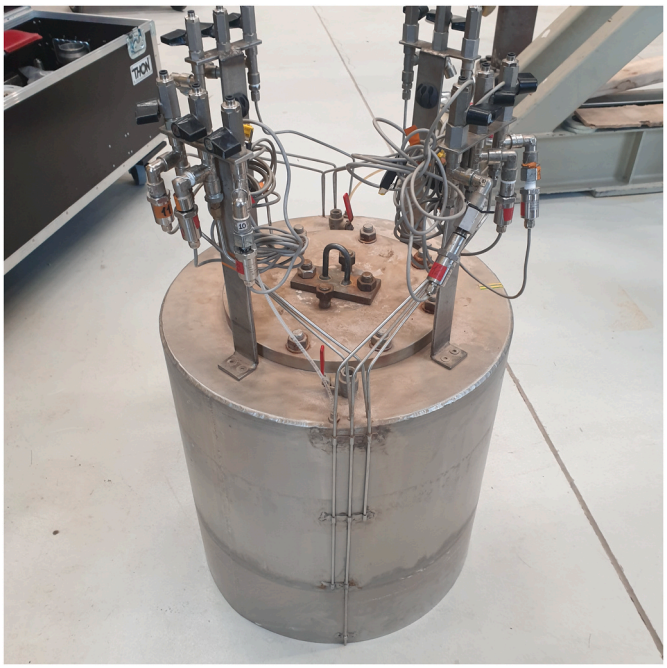

Fig. 3. Photograph of the bucket model.

and are arranged in two diametrically opposite groups of six transducers each.

Fig. 4 illustrates the locations of points for pressure readings. Transducer names refer to their positions in relation to bucket and skirt sides, as well as levels. For example, "LI2" means "left half–inner side–level 2".

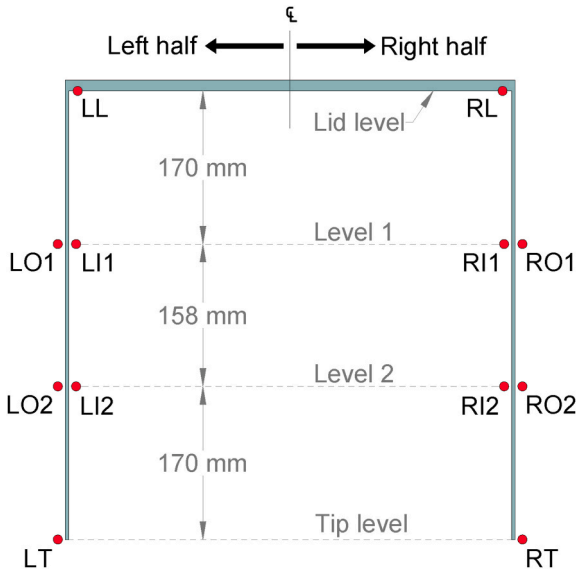

Fig. 4. Positions of pressure reading points.

2.3. Soil characteristics

The sand layer consists of Baskarp Sand no. 15. Its properties are described in Ibsen and Bødker (1994) and outlined in Table 2. The grain distribution is shown in Fig. 5.

Relative density (D_r) constitutes one of the variables in the experimental campaign, as it varies across tests. For the sake of good order, the soil is classified in three categories: loose ($D_r \leq 50$ %), medium (50 % $< D_r \leq 70$ %), and dense ($D_r > 70$ %). It is noted that these terms are established only as a guide for distinguishing soil states in the current study and do not follow any classification convention. The distributions of D_r derived from CPT results aggregated from all 23 tests is presented in Fig. 6. Details on CPT and relative density follow in Section 3.

The distribution related to dense sand appears bimodal, i.e. two peaks emerge at 76% and 83%. The CPTs show higher density inside and around the model area compared to tank boundaries. This is a consistent trend that spans across all tests that involve dense sand and is mirrored by the peaks. Loose sand seems the most uniform, while the opposite is true for medium sand. These outcomes generally reflect the precision and accuracy of the adopted techniques for achieving target densities. It was straightforward to obtain extreme values, whereas the middle range proved more challenging.

3. Testing procedures and program

The methods behind achieving and evaluating the target soil states are briefly outlined here. This is followed by a detailed description of all steps that constitute a test — from model installation until extraction. The section ends with an overview of the testing campaign.

3.1. Soil preparation and CPT

A vibrating rod was used for compaction. It was necessary to insert the rod vertically by hand at 88 equally spaced points covering the entire area to ensure homogeneity, since the volume of soil affected by the rod is relatively small. In some cases, multiple rounds were required. On the other hand, loosening was carried out by progressively inserting a hose with running water at discrete locations and depths.

Between 4 and 8 CPTs were performed prior to installation as part of every test. The sampling locations spanned across the entire soil surface. The resistance (q_c) of a mini-cone with a radius of 7.5 mm and pushed at a rate of 5 mm/s formed the basis for deriving the relative density. Ibsen et al. (2009) calibrated the mini-cone using Baskarp Sand no. 15 and established the relationship between q_c and D_r. This expression, when combined with the definitions of D_r, in situ effective vertical stress (σ'_{vo}) and effective unit weight (γ') takes the form of Eq. (1):

$$\frac{e_{max} - e}{e_{max} - e_{min}} = 0.0514 \left(\frac{\sigma'_{vo}}{q_c^{0.75}} \right)^{-0.42} \tag{1}$$

$$\sigma'_{vo} = \gamma' z = \frac{G_S - 1}{1 + e} \gamma_w z \tag{2}$$

Table 2
Properties of Baskarp Sand no. 15.

Parameter name (Symbol)	Value	Unit
Maximum void ratio (e_{max})	0.854	–
Minimum void ratio (e_{min})	0.549	–
Grain diameter, 50th percentile (d_{50})	0.14	mm
Uniformity coefficient (d_{60}/d_{10})	1.78	–
Specific gravity (G_S)	2.64	–

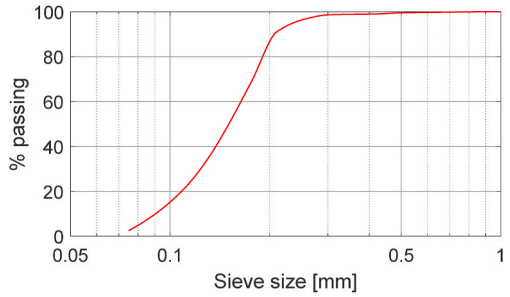

Fig. 5. Particle size distribution of Baskarp Sand no. 15 (data from Borup and Hedegaard, 1995).

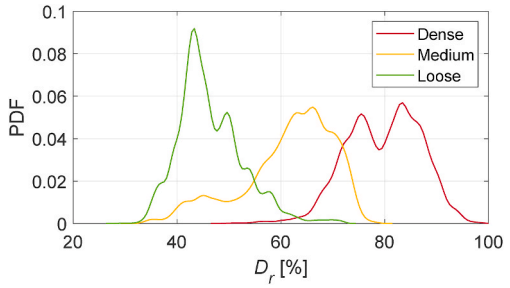

Fig. 6. Distribution of D_r values in each density category.

where e — void ratio, z — depth below soil surface, and γ_w — unit weight of water. Both σ'_{vo} and q_c must be inserted in MPa. By solving Eq. (1) for e, it is possible to further determine all remaining unknowns.

A grand total of 150 CPTs were carried out throughout the whole program. Fig. 7 displays several typical cone resistance profiles, grouped by soil density. The data are affiliated with three tests, each representing a density category. Namely, these are tests no. 2, 7, 22 in Table 3.

3.2. Test phases

Once the CPTs show that the soil state falls into the intended density category, installation and subsequent loading of the model can be undertaken. The structure of a test is described in Fig. 8.

All phases are highlighted in the following list, where item numbers correspond to phase numbers.

(1) *Installation.* The model is installed by pressing it into the soil, with no assistance by means of suction. During this process, the displacement rate is 0.5 mm/s and the lid valves are open, so that entrapped air and water can run out freely without generating pressure build-up, which could alter the initial state of sand. At the start of installation, the model hangs in the air and the load cell reads −0.64 kN, which confirms successful calibration. A sudden increase of resistance indicates initiation of contact between lid and soil surface. The installation procedure ends upon full contact.

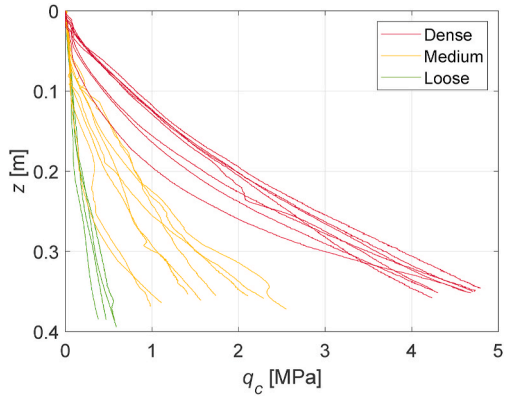

Fig. 7. Cone resistance from selected tests.

Table 3
Overview of the experimental campaign.

Test no.	Test ID	$\overline{D_r}$ [%]	*SD* [%]	*v* [mm/s]
1	L005	52.2	9.4	0.05
2	L10	44.1	3.8	10
3	L50	45.6	5.8	50
4	L150	47.5	5.1	150
5	L500	45.2	5.5	500
6	M005	60.2	7.1	0.05
7	M10	58.5	7.4	10
8	M50	60.1	9.3	50
9	M150a	67.9	6.7	150
10	M150b	57.3	9.2	150
11	M500	66	5.5	500
12	D005	70.7	4.3	0.05
13	D5	75.2	3.1	5
14	D10	80.3	5.2	10
15	D20	76.1	6.2	20
16	D50	80.6	6.6	50
17	D80	78.9	6.9	80
18	D100	80.1	8.6	100
19	D150	80.1	5.3	150
20	D200	77.6	6.8	200
21	D300	80.2	5.4	300
22	D400	80.2	4.3	400
23	D500	75.8	5.6	500

(2) *Pressurization.* The tank is sealed and air is pumped into it until the gauge pressure reaches 200 kPa, which corresponds to an absolute ambient pressure of 300 kPa. This simulates conditions under a 20 m water column.

(3) *Ramp.* This step comes as a necessity to accommodate the specifics of the actuator. The load is set to develop linearly towards the mean cyclic force over a period of 10 min, thus avoiding extreme pore pressure generation.

(4) *Pre-shearing.* The aim of this stage is to simulate the bedding-in process that would occur in field conditions between installation and any significant event (Andersen, 2015; Bienen et al., 2018; Cathie et al., 2019). To this end, 1000 one-way regular compressive load cycles are applied with a frequency of 0.1 Hz. The maximum force within a cycle is defined as 27 kN, which represents 5% of the compressive capacity estimated in accordance with Barari et al. (2017). A similar approach was adopted by Nielsen et al. (2017).

(5) *Dissipation.* A short waiting time is taken in order to let excess pore pressure dissipate. The idea is to extract the model when there is no prior excess pore pressure. This guarantees that all tests start under identical initial conditions, except for uplift rate and soil density.

(6) *Pullout.* The bucket is pulled out at uplift rates that vary between tests. Data acquisition continues for 10 s after complete extraction to allow the estimation of plug weight.

3.3. Program

All experiments and the corresponding values of the independent variables are summarized in Table 3, where $\overline{D_r}$ is the overall mean of samples of relative density, *SD* is the standard deviation of said samples, and *v* is the uplift rate. The test identification is a compound of a letter and a number, which denote the density category and uplift rate in mm/s, respectively. For example, “D5” stands for a test where the sand was dense and the uplift rate was 5 mm/s.

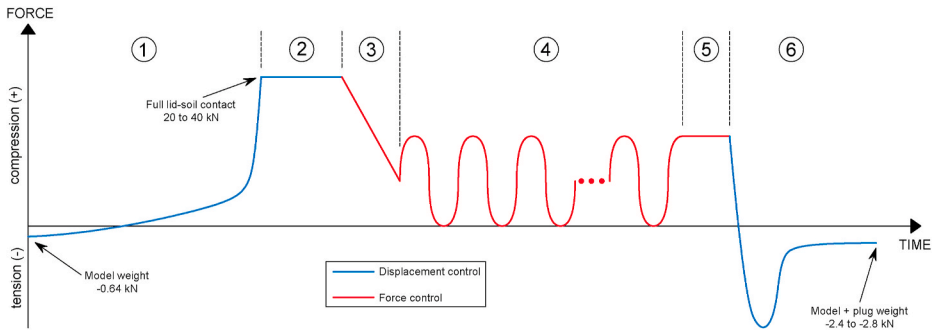

Fig. 8. Schematic of load cell readings during all phases of a test. Dimensions are not to scale.

4. Results and discussion

This section focuses on the results from pullout phases. Tension and upward displacements have negative signs, while the opposite applies to compression and downward displacements. A change of load sign from positive to negative happens in every pullout phase shortly after the model begins displacing (see Fig. 8). However, the positive part, which denotes compressive loading, does not appear in subsequent figures, since only the tensile response is of research interest here.

The processing of raw force data consists of introducing offsets to account for the submerged model weight and the effect of pressurization on the load cell. This is expressed as $= F_{raw} - W_m^{'} - F_{press}$; where F — processed force readings, F_{raw} — raw force readings, $W_m^{'}$ — submerged model weight (−0.567 kN) and F_{press} — pressurization effect on load cell measurements (2.32 kN). All following force results are presented in terms of F. Vertical displacement (u_z) appears in its normalized form as u_z/D_o.

Gütz (2020) points out that the lower and upper bounds of tensile capacity are associated with the drained and undrained conditions, respectively. It is further noted that investigating both conditions is relevant, despite the fact that the field behavior is expected to lie mostly in between the two extremes. Thus, the current study considers the full spectrum of drainage conditions to obtain a complete picture of possible foundation responses.

4.1. Drained conditions

Tests L005, M005, and D005 serve the purpose of assessing the drained tensile resistance (R_t^d) of the foundation model. Drained conditions were ensured by (a) setting a very slow upward displacement rate of 0.05 mm/s and (b) keeping the lid valves open, so that surrounding water could flow freely into the gap between the lid and soil surface. All pressure transducers showed little to no excess pore pressure build-up, proving the success of the adopted methods.

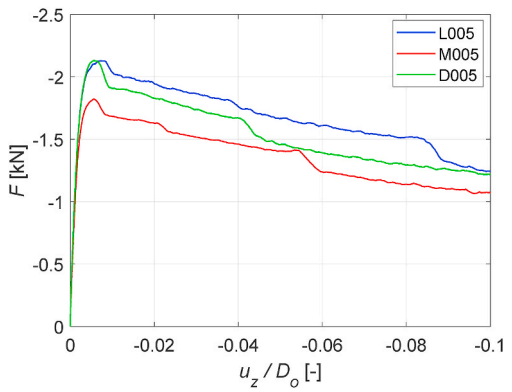

Fig. 9. Load–displacement curves from tests conducted in drained conditions.

Fig. 9 presents the load–displacement curves from drained tests, where it appears that R_t^d ranges from −1.8 to −2.1 kN. Density has no discernible effect given drained conditions, as equal capacities resulted from loosest and densest states, while the one in medium sand is lower. The full mobilization of resistance took place at $u_z/D_o \approx -0.005$ in all three tests.

During drained uplift, tensile resistance is generated solely by friction between soil and skirt. It decreases linearly after reaching the peak value, which indicates proportionality to the area of soil–structure contact. The sudden single drops correspond to the moments when the lid was coming out of water. The distance between lid and water surface varied among tests, which is confirmed by the different positions at which the force drops occurred.

Frictional capacity of bucket foundations can be estimated theoretically using Eq. (2), as given by Larsen et al. (2013):

$$R_t^d = -\pi \frac{\gamma' h^2}{2} \left[(K \tan \delta)_i D_i + (K \tan \delta)_o D_o \right] \quad (3)$$

where h — embedment depth, K — coefficient of lateral earth pressure, and δ — interface friction angle. This approach ignores the reduction of vertical stress close to the skirt (Houlsby et al., 405 2005). The products $(K \tan \delta)_i$ and $(K \tan \delta)_o$ refer to the inner and outer skirt side, respectively. Given the absence of measurements of lateral pressure, it is assumed that $(K \tan \delta)_i = (K \tan \delta)_o$, which makes $(K \tan \delta)$ the only unknown in Eq. (2) and allows its back-calculation. In their empirical analysis of installation of suction buckets in Baskarp Sand no. 15, Rodriguez et al. (2022) found that $\delta \approx 30^\circ$ regardless of soil state. This may bring noteworthy design implications, as it allows explicit evaluation of K and its deviation from the initial value. Using $\delta \approx 30^\circ$ yields $K = 0.93$ as the average result of all three drained tests.

4.2. Undrained and partially drained conditions

Drainage conditions depend on foundation geometry, loading rate, soil permeability and pore fluid viscosity. Additional effects might come from the impermeable soil domain boundaries, i.e., the pressure tank edges. Considering the complex interaction between all the aforementioned factors, the occurrence of the undrained condition can be determined only empirically. This motivated the establishment of a procedure that fulfilled two purposes: (a) finding the minimum v that triggers undrained uplift; (b) enabling the study of the influence of v on the tensile response. The procedure consisted of increasing the uplift rate on a test-by-test basis until the difference between any two consecutive tests became insignificant. It was chosen to conduct this study in dense sand, as it is the most representative state for offshore soil conditions.

The dependency of resistance on uplift rate becomes evident in Fig. 10(a). The difference in force between tests is not directly proportional to the increment in velocity, suggesting a nonlinear relationship. As velocity increases, the tensile response tends asymptotically toward a theoretical maximum, which might be affiliated to the undrained state.

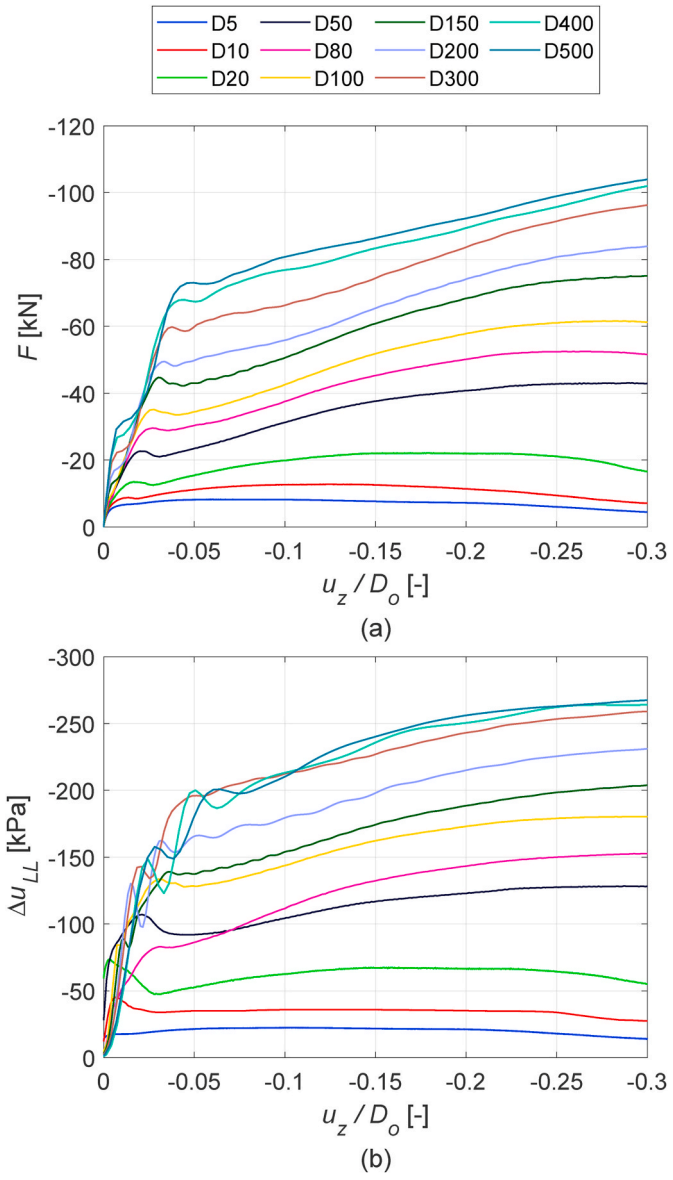

Fig. 10. Outcome of tests performed in dense sand: (a) load–displacement curves; (b) excess pore pressure beneath the lid, as measured by transducer LL.

Despite a relatively large velocity increment of 100 mm/s between D400 and D500, the outcomes thereof appear almost identical. This governed the decision not to apply uplift rates higher than 500 mm/s. The results are shown until $u_z/D_o \approx -0.3$, because this marks the position where the model's lid breaks the water surface. Measurements beyond this point are excluded from the analysis.

Comparing the development of force (Fig. 10(a)) with that of excess pore pressure beneath the lid (Fig. 10(b)), it is noted that strong correlation exists between the two trends. F and Δu_{LL} have a correlation coefficient of almost 1, which implies that suction dictates tensile resistance linearly. In D300, D400, and D500, the excess pore pressures attain similar values, further confirming that an upper limit is reached. This limit appears to fall below the cavitation pressure, which stands at −300 kPa.

Negative excess pore water pressure (Δu) arises on account of two phenomena. The first one relates to the flow of water through a porous medium, since water must seep through soil before reaching a potentially expanding gap between the bucket lid and soil surface. The evolution of Δu is, thus, a time-dependent process, as it links directly to uplift rate and hydraulic conductivity of soil. The second phenomenon comprises the dilative response of sand upon shearing. Ibsen et al. (2009) found that the dilation angle of Baskarp Sand no. 15 at very low confining pressure (≈ 5 kPa) ranges from 12° to 18° for 51 % ≤ D_r ≤ 80 %. The conditions of density and confining pressure coincide with the ones in the current study, which means dilatancy certainly plays a role in the development of Δu.

Under partially drained conditions, the response to uplift relies on suction and skirt friction simultaneously, as explained by Senders (2008). Unlike the drained scenario, inner and outer skirt friction differ by a considerable margin, due to the water flow mechanism triggered by differential pressure. As water seeps into the bucket, a downward hydraulic gradient on the outer side increases the effective stresses, while the opposite effect takes place on the inner side. If the upward gradient inside the bucket reaches a critical value, then the soil plug moves together with the foundation. In this scenario, inner skirt friction reduces by a significant amount and the submerged plug weight becomes a component of resistance. Without accounting for individual contributions of inner and outer friction, the force components can be evaluated based on force equilibrium by means of Eq. (3):

$$F_r = F_f + W_p' = F - F_s \tag{4}$$

where F_r — difference between total and suction force, F_f — friction force, W_p' — submerged soil plug weight, and F_s — suction force, estimated as $F_s = \Delta u_{LL}\pi(D_i/2)^2$. This definition of F_s presumes uniform distribution of Δu over the lid area. Readings from transducer LL, rather than RL, are preferred, since LL proved stable across all tests. Fig. 11 provides a basis for describing how the tensile response evolves with displacement, using examples that are representative of relatively low ($v \leq 50$ mm/s) and high ($v > 50$ mm/s) uplift rates.

At relatively low velocities, the load–displacement curves are characterized by an almost bilinear trend. For example, in test D5, the tangential stiffness remains constant until the failure point at $u_z/D_o \approx -0.005$, after which it approaches zero. Suction is mobilized instantly with displacement, and its magnitude does not change throughout the entire pullout phase. Therefore, the shape of the total response curve is dictated by the frictional component, suggesting that friction governs the failure mechanism. This idea is reinforced by the fact that in drained conditions, which always lead to a purely frictional mechanism, failure occurs at approximately the same displacement.

The tensile response changes in both quantitative and qualitative sense under uplift rates higher than 50 mm/s. In test D500, points A and B denote sudden softening. The change of stiffness at point A comes as a consequence of the actuator's self-stabilization process. Initially, it overshoots the target velocity, then it tends to compensate by decelerating, thereby causing undershooting. The instantaneous velocity converges to the target as soon as the full stabilization cycle ends. This

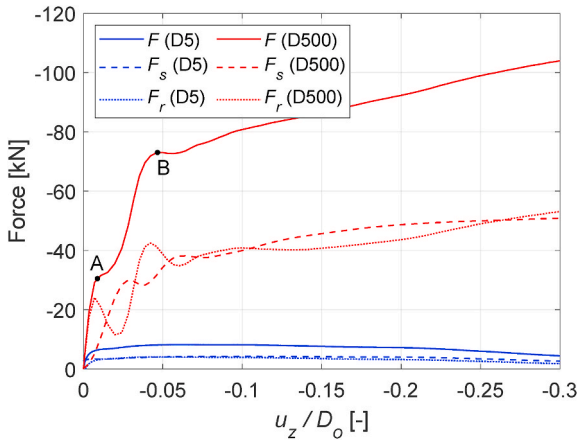

Fig. 11. Force components from selected tests.

behavior of the actuator directly reflects upon the tensile response, since uplift rate and excess pore pressure are highly correlated time-dependent variables. Thus, the first local peak in suction force constitutes an effect of the stabilization cycle.

The occurrence of the local peak at point B may be attributed to the actual mechanics of the foundation system, as the piston rod travels at a steady velocity by that point. The load magnitude at point B is taken as the tensile capacity (R_t) of the bucket, even though it steadily increases further with displacement. The stiffness reduction clearly indicates a change of mechanism. It is hypothesized that this represents the moment of plug mobilization, i.e., when the upward hydraulic gradient reaches the critical value and causes plug heave. Post-test visual inspections revealed that a plug was always extracted with the bucket, regardless of the applied uplift rate. Moreover, the plug volume (V_p) was approximately equal to the volume delimited by the inner bucket surface (V_m), meaning that the plug had moved almost in tandem with the structure. Corroborative evidence that $V_p \approx V_m$ is provided by Gütz (2020), who used a physical foundation model of the same dimensions, although it was installed in a different sand, and they performed all tests at atmospheric pressure. By measuring the plug heave, they found that at an uplift rate of 9.6 mm/s, the ratio between plug and model displacement approached unity. Indeed, this seems to be the case at even lower uplift rates in the present study.

Another insight from Fig. 11 is that the suction force accounts for approximately half of the tensile load. Referring to Eq. (3), the other half relies mostly on friction, as the submerged plug weight (W_p') contributes with only −1.09 kN on average in all tests, regardless of the initial relative density.

As mentioned in Section 3.2, data is acquired for 10 s at the end of the pullout phase, when the bucket hangs freely in the air. This allows to determine the plug weight directly from the load cell readings. Alternatively, the plug weight before the test can be evaluated using the CPT-derived unit weight of the soil. Comparing the estimations related to pre- and post-testing, it is noted that, on average, the plug weight increases by 16%, which translates to densification as a result of applied loading.

The conclusions drawn on the basis of results from experiments conducted in dense sand also hold true in cases that involve looser soil states. This becomes evident upon examining Fig. 12, where load and excess pore pressure beneath the lid are plotted against displacement.

In general, the discrepancies seem relatively insignificant and independent of density, except for tests where $v = 500$ mm/s. In those tests, the differences in Δu are significant, however, their effects on F are rather disproportional. Particularly, Δu in L500 does not follow the typical trend observed in high velocity tests. The readings of transducer LL suggest that the excess pore pressure had not dissipated prior to the pullout phase and that cavitation had occurred. Transducer RL, on the other hand, remained insensitive, which might be explained by potential blockage of the tube connecting the transducer with the lid (see Fig. 3). The only indication of dependency of Δu on sand density is during initial loading, where it appears that Δu builds up at a higher rate in loose sand. This aligns with the conclusions of numerical studies presented by Gao et al. (2021, 2022).

The load–displacement curves in Fig. 12(a) appear nearly identical. There is no observable consistent trend that would indicate a relationship between the tensile response and relative density. This might be attributed partly to densification due to jacking installation, as quantitatively described by Rodriguez et al. (2022). Another potential reason relates to the cyclic pre-shearing procedure, during which net downward displacement occurred. Consequently, the soil density in proximity to the bucket might have attained similar values at the end of pre-shearing in all tests.

4.3. Influence of pre-shearing

A single control test was conducted to study the influence of pre-shearing. In this test, the foundation was subjected to uplift immediately following the installation, thus essentially skipping phase 3 and 4 (see Fig. 8). The characteristics of test D150 from the main program were replicated so that the presence of pre-shearing became the only variable.

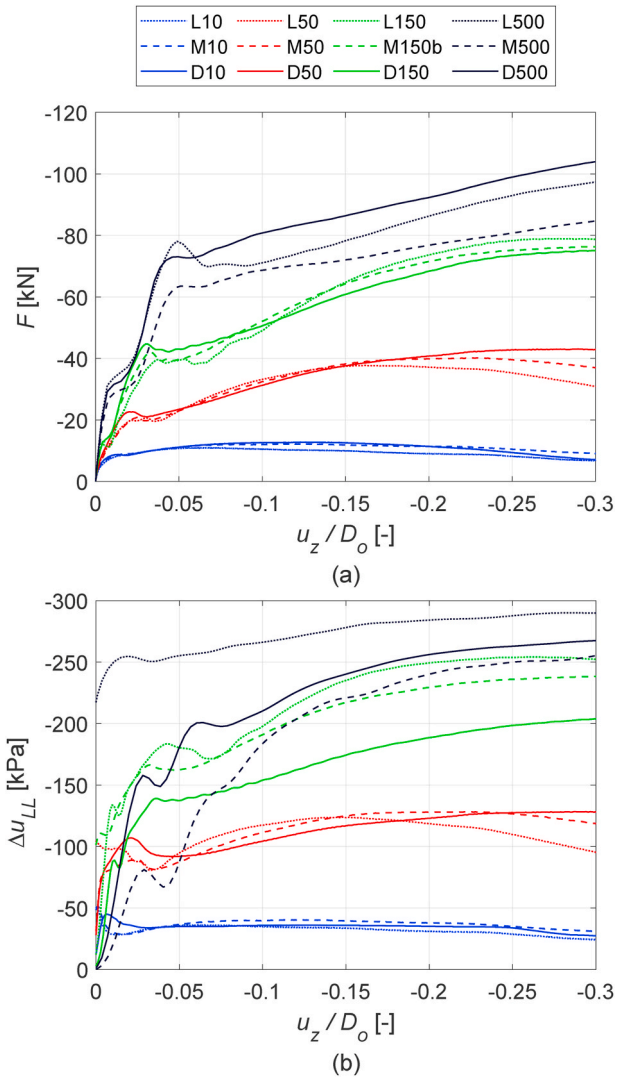

Fig. 12. Outcome of tests performed in loose, medium, and dense sand: (a) load–displacement curves; (b) excess pore pressure beneath the lid, as measured by transducer LL.

Fig. 13 highlights significant differences between tests, except until the velocity stagger, which was described previously in Section 4.2. Pre-shearing contributed to increased stiffness before failure. On the other hand, the response appears generally softer in presence of undisturbed sand, with no clearly defined failure point. Although higher tensile capacity was ultimately achieved, it took considerably larger displacements.

In a similar study at a smaller scale, Kelly et al. (2006) noted degradation of both stiffness and capacity in tests where pre-shearing had been applied. The current results confirm this phenomenon, although a slightly stiffer pre-failure response occurs as a consequence of cycling. The development patterns and magnitudes of F in Fig. 13 are largely dictated by excess pore pressure. With no pre-shearing, Δu inside the bucket reached the cavitation pressure of −300 kPa, while a maximum of −200 kPa was measured in the other test. A potential cause is that cycling had induced enough plastic straining to reduce the available strength to some residual level prior to uplift. In such case, less

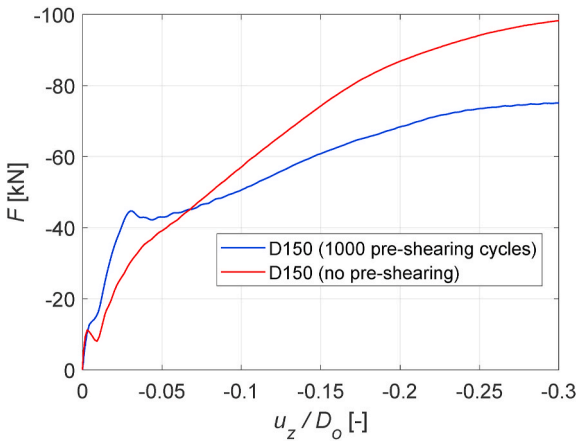

Fig. 13. Dependency of tensile response on application of pre-shearing cycles.

suction would be required to fully engage the failure mechanism.

4.4. Excess pore pressure

It is clear from the above discussion that excess pore pressure plays a major role in tensile response development under rapid loading. The seepage mechanism generated by uplift is well-documented and generally understood, and the empirical evidence obtained here supports the findings of, e.g., Gourvenec and Randolph (2010), Koteras and Ibsen (2019), Lai et al. (2022). Fig. 14 shows the evolution of Δu at multiple points over the model surface. See Fig. 3 for a reminder on sampling locations.

The excess pore pressure beneath the lid gains significant magnitude at the onset of displacement. However, responses come with certain delays deeper along the skirt. This behavior, which can be characterized by a pressure front traveling downwards, was also observed by Kelly et al. (2006). A common outcome of all tests is that the Δu values across all sampling points inside the bucket eventually become almost equal, suggesting that a uniform pore pressure distribution was always reached and sustained. The displacement at which this happens depends on the uplift rate, among other factors such as seepage length and hydraulic conductivity.

Under 10 mm/s, disparities between readings disappear at a smaller u_z than they do under 500 mm/s. The pressure front managed to cover the entire inner bucket volume before the water surface was reached at $u_z/D_o \approx -0.3$ in all tests. The head isochrones in Fig. 15 reveal that uniform states were attained after 5 s and 0.25 s in D10 and D500,

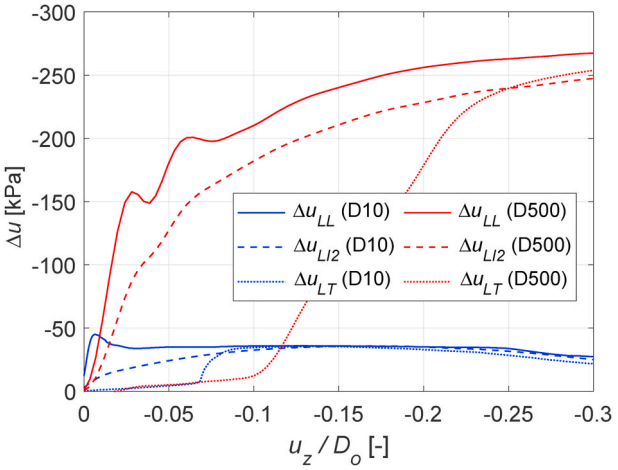

Fig. 14. Pore pressure readings at different depths along the inner skirt side.

respectively. This indicates that the process of pressure equalization strongly depends on the intensity of applied loading.

The circular markers in Fig. 15 represent readings from transducers. The general distribution of Δu along the skirt can be visualized, despite the absence of some data that is deliberately discarded due to transducer malfunctions. On the outer side, pressure builds up rapidly with distance to the tip, forming a gradient that persists until loading ends. This is not the case on the inner side, where the gradient essentially disappears after certain amounts of time, depending on uplift rate. The absence of a gradient, that is, Δu is equal at all points along the skirt, may be interpreted as an indicator of fully undrained conditions (Vaitkunaite et al., 2016). Expanding on this idea, the magnitude of the gradient may serve as base for quantifying the degree of drainage state. However, the development of a corresponding methodology falls out of the scope of this study.

5. Regression models

The dependency of tensile capacity (R_t) and initial stiffness (K_i) on uplift rate (v) and relative density (D_r) is studied here. The intention is to define models that are valid exclusively within the ranges of investigated variables, since the results cannot be extrapolated without further empirical evidence. Furthermore, the scope of application is limited to bucket foundations of $L/D = 1$ and sandy soils. The effects of various cyclic loads and suction-assisted installation prior to uplift are not incorporated in the models.

The regression analysis omits four tests, since they exhibit features that set them apart from the rest. Test L500 is the only one where cavitation occurred, as indicated by pressure readings of −300 kPa. In contrast, drained tests L005, M005, and D005 are characterized by almost zero excess pore pressure.

5.1. Dimensionless groups

Variables are combined to form dimensionless groups, thereby ensuring dimensional homogeneity. Table 4 presents all combinations. The force–length–time (FLT) system is used.

The estimations of initial hydraulic conductivity (k_0) of Baskarp Sand no. 15 are based on results from a series of falling head tests performed by Sjelmo (2012). Eq. (4) represents the outcome of those tests:

$$k_0 = p_1 e^2 + p_2 e + p_3 \tag{5}$$

where e — void ratio, $p_1 = 8.82 \times 10^{-4}$ m/s, $p_2 = -7.36 \times 10^{-4}$ m/s, and $p_3 = 1.96 \times 10^{-4}$ m/s.

5.2. Tensile capacity

The load magnitude at point B in Fig. 11 is interpreted as the tensile capacity. Figs. 16 and 17 aggregate the results from all tests that are part of the regression analysis. Comparing the two figures, it becomes evident that D_r influences R_t to a significantly lower degree than v. No trend can be discerned when inspecting Fig. 16, therefore D_r is not included as an explanatory variable in the model.

The fitted curve in Fig. 17 is a power function found as:

$$\frac{R_t}{\gamma' D_o^3} = A\left(\frac{v}{k_0}\right)^B \tag{6}$$

where $A = -1.018$ and $B = 0.4634$; with $R^2 = 0.98$. This model incorporates the idea that R_t is related directly to v and inversely to k_0, which is consistent with the physics of system. A combination of high uplift rate and low permeability leads to a large resistance on account of suction force, while the opposite holds true as well. Eq. (5) links R_t with foundation geometry (D_o), loading characteristics (v), and soil properties (γ', k_0). A limitation of the model appears when $v \approx k_0$, that is

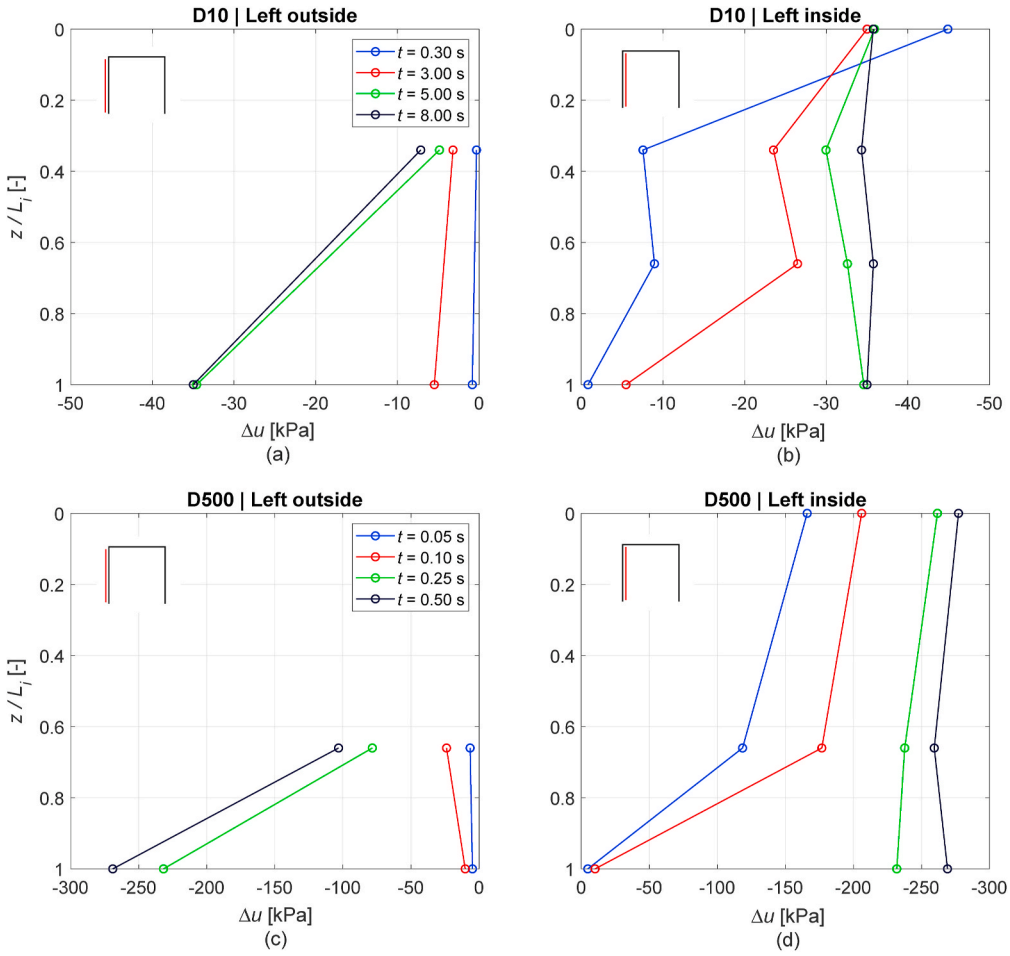

Fig. 15. Excess pore pressure distribution at selected instances of time.

Table 4
Groups of variables.

Name (Symbol)	Group	Dimension
Tensile capacity (R_t)	$R_t/(\gamma' D_o^3)$	$F/(FL^{-3}L^3)$
Initial stiffness (K_i)	$K_i/(\gamma' D_o^2)$	$FL^{-1}/(FL^{-3}L^2)$
Uplift rate (v)	v/k_0	$LT^{-1}/(LT^{-1})$

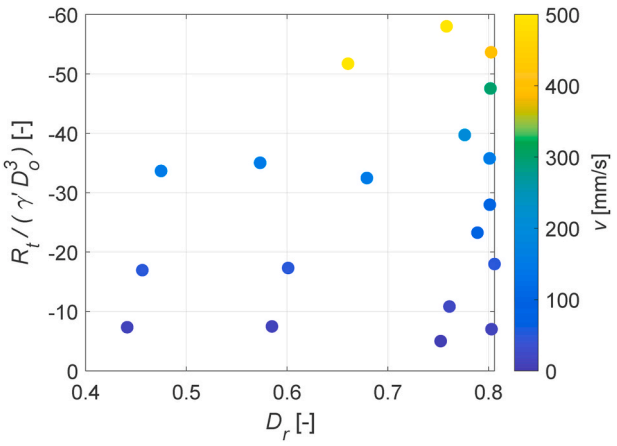

Fig. 16. Tensile capacity against relative density.

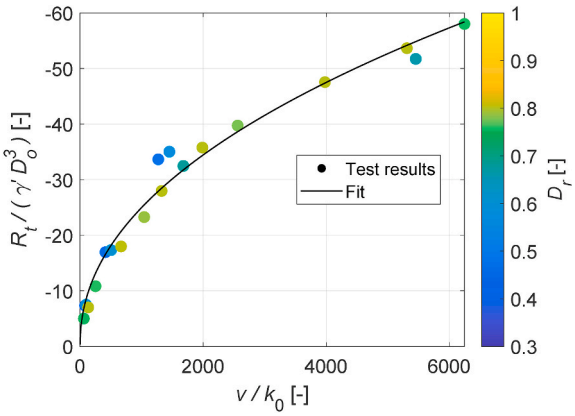

Fig. 17. Tensile capacity against uplift rate.

$v/k_0 \approx 1$, as it implies low R_t regardless of the absolute values of v and k_0. In other words, the model treats rapid pullout in very permeable sand and slow pullout in less permeable sand as identical scenarios. However, $v/k_0 \approx 1$ lies beyond the domain within which the model is formulated ($62 \leq v/k_0 \leq 6247$), and thus does not represent a valid input.

5.3. *Initial stiffness*

Initial stiffness, which reflects the effects of jacking installation and pre-shearing, is defined as the slope of the line $y = \kappa x$ fitted to all data

points until $u_z/D_o = -0.01$. As before, K_i values from all tests are plotted against the independent variables in Figs. 18 and 19.

Again, no strong dependency of K_i on D_r is apparent. On the contrary, there seems to exist a clear trend between K_i and v. A piecewise function is used to describe this relationship:

$$\frac{K_i}{\gamma' D_o^2} = \begin{cases} C_1 \left(\frac{v}{k_0}\right)^{C_2} & \text{for} \quad \frac{v}{k_0} \leq \alpha \\ C_1(\alpha)^{C_2} + C_3\left(\frac{v}{k_0} - \alpha\right) & \text{for} \quad \frac{v}{k_0} > \alpha \end{cases} \tag{7}$$

where $C_1 = 347$, $C_2 = 0.2047$, $C_3 = 0.4685$, and $\alpha = 2000$; with $R^2 = 0.95$. The models of K_i and R_t resemble each other in shapes, variables, and limitations. Therefore, the description provided at the end of Section 5.2 also applies here.

6. Conclusions

A set of tests were conducted on a suction bucket model in a pressurized environment, where the additional ambient pressure was 200 kPa to simulate 20 m of water depth. The model was subjected to monotonic pullout at uplift rates varying from 0.05 mm/s to 500 mm/s in loose, medium, and dense sand. This allowed the observation of tensile responses under the complete range of drainage conditions: from drained to undrained. The main conclusions of the experimental campaign are listed as follows:

- The uplift rate influenced the tensile response by a significantly higher degree than soil density. The development of negative excess pore pressure, which translates to resistance on account of suction beneath the lid, appears more sensitive to loading characteristics than to sand properties. The effects of density may have been partly diminished due to (1) densification affiliated with jacking installation, and (2) pre-shearing prior to pullout, as the one-way compressive force cycles always caused net downward displacement. This means that, potentially, at the start of each pullout, the relative density within the bucket volume was approximately the same. There were no means to assess density during testing.
- As expected, strong correlation between the tensile response and suction became evident. Suction accounted for about half of tensile resistance, which is somewhat lower compared to similar studies. Once again, it is confirmed that increased resistance comes at the cost of relatively large displacements required for its mobilization.
- A regression model was established to capture the non-linear dependency of tensile capacity and initial stiffness on uplift rate. The model incorporates foundation geometry, soil properties, and loading characteristics.
- A full soil plug was mobilized in all tests, except under drained conditions. The force readings at the end of each test suggest that densification had occurred.
- The development of excess pore pressure follows a consistent trend, highlighted by a delay between pressure beneath the lid and skirt tip. Uniform pressure distribution inside the bucket was always eventually reached, but it happened at different times, depending proportionally on the applied uplift rate. Cavitation occurred only in one test.
- Applying pre-shearing cycles affects the tensile response characteristics notably. It led to lower capacity on account of smaller suction force, in comparison to a test where no cyclic pre-shearing was involved. Moreover, pre-shearing appears central in causing the almost bilinear trend in load–displacement curves, where a distinct point of softening is present. A separate study would be required to assess the impact of various pre-shearing characteristics.

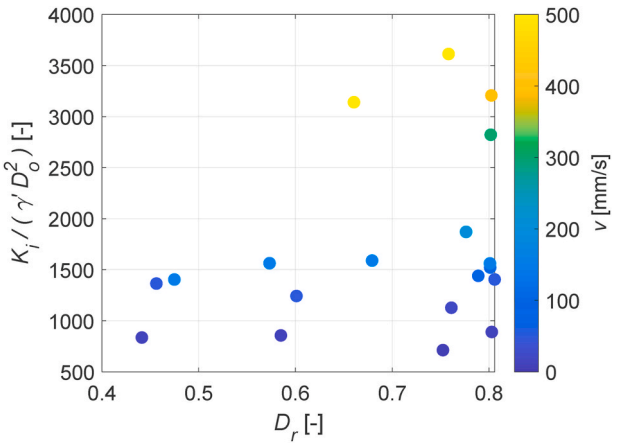

Fig. 18. Initial stiffness against relative density.

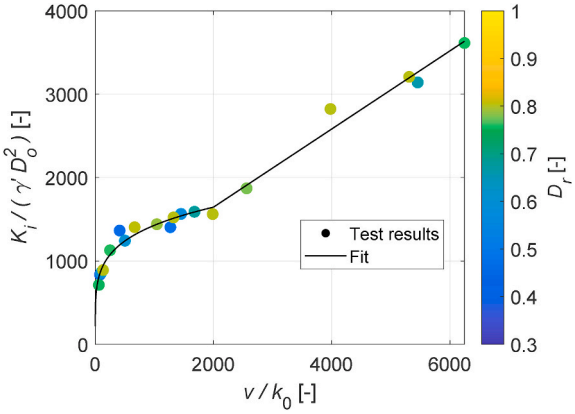

Fig. 19. Initial stiffness against uplift rate.

CRediT authorship contribution statement

Sorin Grecu: Conceptualization, Methodology, Software, Validation, Formal analysis, Investigation, Data curation, Writing – original draft, Writing – review & editing, Visualization. **Lars Bo Ibsen:** Conceptualization, Methodology, Resources, Writing – review & editing, Supervision, Project administration, Funding acquisition. **Amin Barari:** Conceptualization, Methodology, Writing – review & editing, Supervision.

Declaration of competing interest

The authors declare that they have no known competing financial interests or personal relationships that could have appeared to influence the work reported in this paper.

Data availability

The authors do not have permission to share data.

Acknowledgements

The authors express their gratitude to Carolina, Elena, and Kim for their excellent hard work during all stages of the experimental campaign in the soil laboratory. Furthermore, the authors acknowledge the Department of the Built Environment, Aalborg University, for fully supporting this research through no specific grant.

References

Acosta-Martinez, H.E., Gourvenec, S., Randolph, M.F., 2012. Centrifuge study of capacity of a skirted foundation under eccentric transient and sustained uplift. Geotechnique 62 (4), 317–328.

Acosta-Martinez, H.E., Gourvenec, S.M., Randolph, M.F., 2008. An experimental investigation of a shallow skirted foundation under compression and tension. Soils Found. 48 (2), 247–254.

Andersen, K.H., 2015. Cyclic soil parameters for offshore foundation design. In: Meyer, V. (Ed.), Frontiers in Offshore Geotechnics III – Proceedings of the 3rd International Symposium on Frontiers in Offshore Geotechnics (ISFOG 2015), Oslo, Norway. CRC Press, pp. 5–82.

Barari, A., Ibsen, L.B., Taghavi Ghalesari, A., Larsen, K.A., 2017. Embedment effects on vertical bearing capacity of offshore bucket foundations on cohesionless soil. Int. J. GeoMech. 17 (4), 04016110.

Bienen, B., Klinkvort, R.T., O'Loughlin, C.D., Zhu, F., Byrne, B.W., 2018. Suction caissons in dense sand, part I: installation, limiting capacity and drainage. Geotechnique 68 (11), 937–952.

Borup, M., Hedegaard, J., 1995. Baskarp Sand No. 15: Data Report 9403. Aalborg University.

Byrne, B.W., Houlsby, G.T., 2002. Experimental investigations of response of suction caissons to transient vertical loading. J. Geotech. Geoenviron. Eng. 128 (11), 926–939.

Cathie, D., Irvine, J., Houlsby, G., Byrne, B., Buykx, S., Dekker, M., Jansen, E., Dijkstra, O.J., Schuhmacher, T., Morgan, N., 2019. Suction installed caisson foundations for offshore wind: design guidelines. https://www.carbontrust.com/resources/guidelines-for-the-design-of-suction-caisson-foundations-for-offshore-wind-farms. (Accessed 14 October 2022) accessed.

Chen, W., Randolph, M.F., 2007. Uplift capacity of suction caissons under sustained and cyclic loading in soft clay. J. Geotech. Geoenviron. Eng. 133 (11), 1352–1363.

Gao, B., Ye, G., Zhang, Q., Xie, Y., Yan, B., 2021. Numerical simulation of suction bucket foundation response located in liquefiable sand under earthquakes. Ocean. Eng. 235, 109394.

Gao, B., Zhu, W., Zhang, Q., Ye, G., 2022. Response of suction bucket foundation subjected to wind and earthquake loads on liquefiable sandy seabed. Soil Dynam. Earthq. Eng. 160, 107338.

Gourvenec, S., Randolph, M.F., 2010. Consolidation beneath circular skirted foundations. Int. J. GeoMech. 10 (1), 22–29.

Grecu, S., Ibsen, L.B., Barari, A., 2021. Winkler springs for axial response of suction bucket foundations in cohesionless soil. Soils Found. 61 (1), 398 64–79.

Gütz, P., 2020. Tensile Loaded Suction Bucket Foundations for Offshore Structures in Sand. PhD Thesis. Leibniz University, Hannover.

Gütz, P., Achmus, M., Thieken, K., Schröder, C., 2017. Model testing of suction bucket foundations under tensile loading in non-cohesive soil. In: Proceedings of the 8th International Conference on Offshore Site Investigation and Geotechnics. Society of Underwater Technology, London, UK, pp. 578–585.

Hansteen, O., Jostad, H., Tjelta, T.I., 2003. Observed platform response to a "monster" wave. In: Myrvoll, F. (Ed.), Field Measurements in Geomechanics. A.A. . Balkema Publishers, pp. 73–86.

Houlsby, G.T., Kelly, R.B., Byrne, B.W., 405 2005. The tensile capacity of suction caissons in sand under rapid loading. In: Gourvenec, S., Cassidy, M. (Eds.), Frontiers in Offshore Geotechnics I - Proceedings of the 1st International Symposium on Frontiers in Offshore Geotechnics (ISFOG 2005). CRC Press, Perth, WA, Australia, pp. 405–410.

Ibsen, L.B., Bødker, L., 1994. Baskarp Sand No. 15: Data Report 9301. Aalborg University.

Ibsen, L.B., Hanson, M., Hjort, T., Thaarup, M., 2009. MC-parameter Calibration of Baskarp Sand No. 15: DCE Technical Report No. 62. Aalborg University.

Jeong, Y.H., Kim, J.H., Manandhar, S., Ha, J.G., Park, H.J., Kim, D.S., 2020. Centrifuge modelling of drained pullout and compression cyclic behaviour of suction bucket. Int. J. Phys. Model. Geotech. 20 (2), 59–70.

Kakasoltani, S., Zeinoddini, M., Abdi, M.R., Arabzadeh, H., 2011. An experimental investigation into the pull-out capacity of suction caissons in sand. In: Proceedings of the ASME 2011 30th International Conference on Ocean. Offshore and Arctic Engineering, Rotterdam, The Netherlands, pp. 21–27.

Kelly, R.B., Byrne, B.W., Houlsby, G.T., Martin, C.M., 2004. Tensile loading of model caisson foundations for structures on sand. In: Proceedings of the 14th International Offshore and Polar Engineering Conference. Toulon, France, pp. 638–641.

Kelly, R.B., Houlsby, G.T., Byrne, B.W., 2006. Transient vertical loading of model suction caissons in a pressure chamber. Geotechnique 56 (10), 665–675.

Koh, K.X., Hossain, M.S., Kim, Y., 2017. Installation and monotonic pullout of a suction caisson anchor in calcareous silt. J. Geotech. Geoenviron. Eng. 143 (2), 04016098.

Koteras, A.K., Ibsen, L.B., 2019. Medium-scale laboratory model of mono-bucket foundation for installation tests in sand. Can. Geotech. J. 56 (8), 1142–1153.

Kulczykowski, M., 2020. Experimental investigation of skirted foundation in sand subjected to rapid uplift. Arch. Hydroeng. Environ. Mech. 67 (1–4), 17–34.

Lai, Y., Chen, C., Zhu, B., Dai, J.l., Kong, D.q., 2022. Numerical modelling on effect of loading rate on uplift behavior of suction caissons. Ocean. Eng. 260, 112013.

Larsen, K.A., Ibsen, L.B., Barari, A., 2013. Modified expression for the failure criterion of bucket foundations subjected to combined loading. Can. Geotech. J. 50 (12), 1250–1259.

Luke, A.M., Rauch, A.F., Olson, R.E., Meham, E.C., 2005. Components of suction caisson capacity measured in axial pullout tests. Ocean. Eng. 32, 878–891.

Mana, D.S.K., Gourvenec, S., Hossain, M.S., Randolph, M.F., 2011. Experimental investigation of the undrained response of a shallow skirted foundation subjected to vertical compression and uplift. In: Proceedings of the ASME 2011 30th International Conference on Ocean. Offshore and Arctic Engineering, Rotterdam, The Netherlands, pp. 771–778.

Mana, D.S.K., Gourvenec, S., Randolph, M.F., 2013a. A novel technique to mitigate the effect of gapping on the uplift capacity of offshore shallow foundations. Geotechnique 63 (14), 1245–1252.

Mana, D.S.K., Gourvenec, S., Randolph, M.F., 2013b. Experimental investigation of reverse end bearing of offshore shallow foundations. Can. Geotech. J. 50 (10), 1022–1033.

Mana, D.S.K., Gourvenec, S.M., Randolph, M.F., Hossain, M.S., 2012. Failure mechanisms of skirted foundations in uplift and compression. Int. J. Phys. Model. Geotech. 12 (2), 47–62.

Nielsen, S.D., Ibsen, L.B., Nielsen, B.N., 2017. Response of cyclic-loaded bucket foundations in saturated dense sand. J. Geotech. Geoenviron. Eng. 143 (11), 04017086.

Rodriguez, F.M.G., Ibsen, L.B., Koteras, A.K., Barari, A., 2022. Investigation of 443 the penetration resistance coefficients for the CPT-BasedMethod for suction bucket foundation installation in sand. Int. J. GeoMech. 22 (6), 04022063.

Senders, M., 2008. Suction Caissons in Sand as Tripod Foundations for Offshore Wind Turbines. PhD Thesis. The University of Western Australia.

Shonberg, A., Harte, M., Aghakouchak, A., Brown, C.S.D., Pacheco Andrade, M., Liingaard, M.A., 2017. Suction bucket jackets for offshore wind turbines: applications from in situ observations. In: Shin, Y. (Ed.), Proceedings of TC 209 Workshop at the 19th ICSMGE: Foundation Design of Offshore Wind Structures, Seoul, South Korea. ISSMGE, pp. 65–77.

Sjelmo, A., 2012. Soil-Structure Interaction in Cohesionless Soils Due to Monotonic Loading. Master's thesis. Aalborg University.

Thieken, K., Achmus, M., Schröder, C., 2014. On the behavior of suction buckets in sand under tensile loads. Comput. Geotech. 60, 88–100.

Tjelta, T.I., 2015. The suction foundation technology. In: Meyer, V. (Ed.), Frontiers in Offshore Geotechnics III — Proceedings of the 3rd International Symposium on Frontiers in Offshore Geotechnics (ISFOG 2015), Oslo, Norway. CRC Press, pp. 85–93.

Vaitkunaite, E., Nielsen, B.N., Ibsen, L.B., 2016. Bucket foundation response under various displacement rates. Int. J. Offshore Polar Eng. 26 (2), 116–124.

Vaitkune, E., Ibsen, L.B., Nielsen, B.N., 2017. Bucket foundation model testing under tensile axial loading. Can. Geotech. J. 54 (5), 720–728.

Vicent, S., Hong, S., Bong, T., Kim, S.R., 2021. Effects of embedment depth on the pullout capacity of bucket foundations in sand. Ocean. Eng. 237, 109643.

Vicent, S., Kim, S.R., Van Tung, D., Bong, T., 2020. Effect of loading rate on the pullout capacity of offshore bucket foundations in sand. Ocean. Eng. 210, 107427.

Wang, L.Z., Wang, H., Zhu, B., Hong, Y., 2018. Comparison of monotonic and cyclic lateral response between monopod and tripod bucket foundations in medium dense sand. Ocean. Eng. 155, 88–105.

Wang, X., Zeng, X., Li, J., 2019. Vertical performance of suction bucket foundation for offshore wind turbines in sand. Ocean. Eng. 180, 40–48.

Zhao, L., Bransby, M.F., Gaudin, C., 2020. Centrifuge observations on multidirectional loading of a suction caisson in dense sand. Acta Geotech 15 (6), 1439–1451.